Viscocapillary Model of Slide Coating: Effect of Operating Parameters and Range of Validity

K. Tjiptowidjojo
Coating Process Fundamentals Program, Dept. of Chemical Engineering and Material Science, University of Minnesota, Minneapolis, MN 55455

M. S. Carvalho
Dept. of Mechanical Engineering, Pontificia Universidade Católica do Rio de Janeiro, Rio de Janeiro, RJ 22453-900, Brazil

DOI 10.1002/aic.11843
Published online July 17, 2009 in Wiley InterScience (www.interscience.wiley.com).

Slide coating is one of the premetered high-precision coating methods. The layer thickness is set by the flow rate and web speed. The uniformity of the layer, however, can be affected by other operating conditions. Modeling the flow in the coating bead is necessary in developing the range of operability conditions where the layer is adequately uniform. Lubrication and viscocapillary models have been used to describe the flow and some of the operability limits of different coating processes. However, the available models of slide coating were developed with adhoc hypotheses that compromise their accuracy. We present a critical review of the available viscocapillary models and proposed changes to improve its range of applicability. The accuracy of the model is tested by comparing its predictions to the solution of the full two-dimensional Navier-Stokes equation. The model is valid at low capillary and Reynolds number regime and at low gap-to-wet thickness ratio. © 2009 American Institute of Chemical Engineers *AIChE J,* 55: 2491–2505, 2009

Keywords: slide coating, viscocapillary model, film flow equation, matching conditions

Introduction

Slide coating is a method for rapidly depositing one or more liquid layers onto a moving substrate simultaneously. This method is commonly used in the manufacturing of photographic products, magnetic recording media, and optical films. Slide coating belongs to a class of coating methods called premetered coating. The thickness of the coating is set by the liquid flow rate and web speed only and it is independent of other process variables, making it the method of choice for precision coating. However, the nature of the flow in the coating bead and therefore the uniformity of the liquid layer deposited on the substrate can be affected by the operating variables. The region in the operating parameters of a coating process where the applied liquid layer is adequately uniform is referred to the coating window. Modeling the flow in the coating bead and its stability limits is an important tool in the development of operability windows of different coating processes.

Many important aspects of coating flows are well accounted for by one-dimensional lubrication and viscocapillary models that are easier to setup, computationally far less expensive to use, and more straightforward to interpret than families of solutions of two-dimensional Navier-Stokes equation system. The latter is generally more accurate and reliable, but requires specialized algorithms to account for the free surface and demands substantial computation time.[1] Youn et al.[2] presented a review of the available viscocapillary models for premetered coating flows. Unlike slot coating, no simple accurate model of even single-layer slide

This article is dedicated to the late Prof. L. E. "Skip" Scriven.

Correspondence concerning this article should be addressed to M. S. Carvalho at msc@puc-rio.br

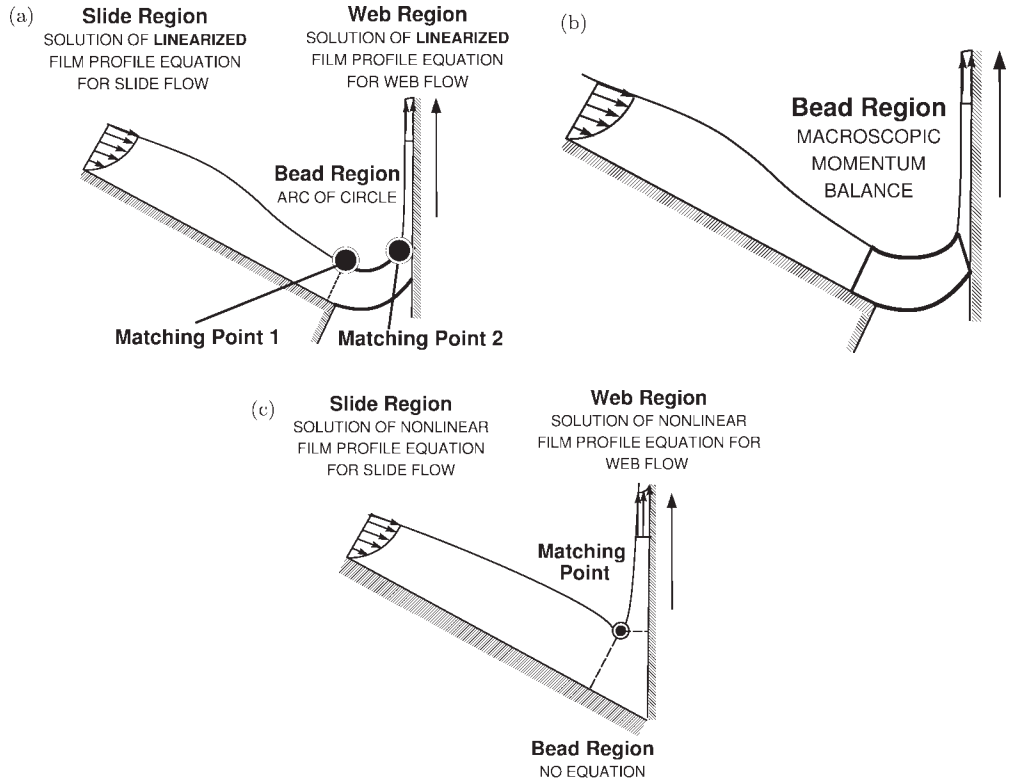

Figure 1. Proposed simple models of slide coating.

(a) Galehouse and Golt[3]; (b) Hens and Van Abbenyem[4]; (c) Nagashima.[5,6]

coating has emerged. We believe that the absence of an accurate model is caused by the less confinement of the liquid by solid surfaces and the nonunidirectional flow at the film formation region.

A viscocapillary model for slide coating flow that ignores inertia and balances viscous force with capillary pressure was presented by Galehouse and Colt.[3] Their model consists of analytical solutions of the linearized film profile equations of flows down an inclined plane and up a moving surface, which are valid approximations only far upstream on the slide and far downstream on the web. The bead that connects these two regions is assumed to be thick enough yet immune to gravity so that its pressure is constant and its upper free surface is an arc of circle. These three parts, slide flow, web flow, and circular bead, are spliced together by requiring inclination and curvature to be continuous at two arbitrarily chosen matching points, as shown in Figure 1a. This model, though crude, is the pioneering attempt at a simple one-dimensional viscocapillary model of slide coating.

Another simple model was proposed by Hens and Van Abbenyen.[4] They focused on neither the arriving film flow on the slide nor the departing flow on the web. Instead, they defined a bead region, as shown in Figure 1b, to construct for it an overall momentum balance by postulating plausible influxes and outfluxes of momentum together with gravitational forces acting on the bead section, pressure ("vacuum") on free surfaces, surface tension at cuts in free surfaces, and most problematic of all, viscous drag on the portions of slide and web that are inside their control volume. The severe limitation is the empiricism of their estimates, above all the appeal to Sakiadis' patently inappropriate boundary layer flow and the disregard of the flow rearrangements in the bead region, including the effect of capillary pressure gradient from varying curvature of the flow's upper free surface. In essence, they postulated solutions of the Navier-Stokes system for viscous free surface flow in the bead without examining critically the then available Navier-Stokes solutions.[1]

Nagashima[5,6] attempted to extend Galehouse and Colt's model to include more of the flow rearrangements in the bead region by not linearizing the film profile equations on the slide and the web and retaining the inertia, i.e., momentum convection, terms in them. However instead of interposing an effectively static bead region in between the one-dimensional slide and web flows as Galehouse and Colt did, he spliced the solution of the slide flow equation with that of web flow equation directly at a plausibly, yet arbitrarily chosen, matching point, as shown in Figure 1c. He did so in the expectation that the viscous and inertial force would become negligible at the matching point so that both equations would describe one and the same nearly static meniscus there. They were not, however, in the parameter ranges which Nagashima examined. So the question remains as to whether there is a parameter range which which one-dimensional models of slide coating is accurate. Another important point is the possibility of improving the one-dimensional models by developing simple yet accurate models of the coating bead region to fit correctly between the nonlinear asymptotic approximations of the flow down the slide and along the web. Jung et al.[7] used similar approach to study a slide-fed

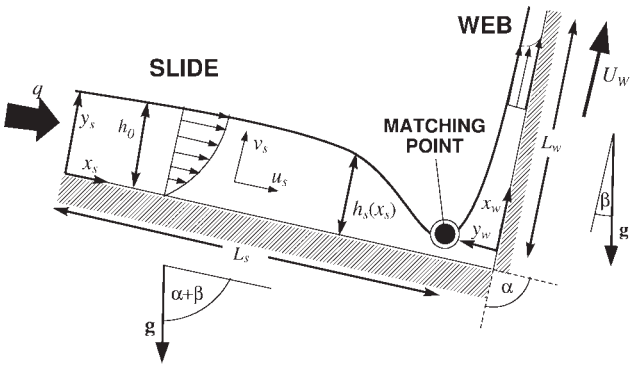

Figure 2. Slide coating flow.

curtain coating process, and the solution of the film profile equation down the slide was matched to the solution of the film profile equation of a free falling liquid curtain.

This work presents a thorough critical examination of the nonlinear asymptotic model for the flow down the slide and up the moving web reported by Nagashima.[5,6] The model is rewritten in terms of an arc length coordinate system defined along the free surface, which avoids singularities that may occur when a Cartesian system is used. Effects of the conditions used to match both film profiles and the way they are imposed in the discrete system is examined. Furthermore, the effect of different operating parameters on the flow and the limits of the process are investigated as well. The range of applicability of the one-dimensional nonlinear model is determined by comparing the predictions to the solution of the complete two-dimensional Navier-Stokes.

Nonlinear Asymptotic Model of Slide Coating Flow

Film profile equation

The film profile equation is an ordinary differential equation that governs the variation of film thickness along a one-dimensional solid support, as illustrated in the case of slide coating flow in Figure 2. The form of the film profile equation depends on the approximations used in simplifying the complete two-dimensional Navier-Stokes equation system. The film profile equation used by Nagashima[5,6] is obtained with the approach outlined by Higgins and Scriven.[8] Similar approach has been used to derive film profile equation to describe the flow in a slide-fed curtain coating process.[7] The fundamental steps of the derivation of film profile equation of the flow down a slide are shown here as an example of the procedure.

First, the Navier-Stokes equation is simplified by assuming the flow down the slide to be locally rectilinear. The simplification leads to the following equations:

$$\frac{\partial u_s}{\partial x_s} + \frac{\partial v_s}{\partial y_s} = 0 \tag{1}$$

$$Re\left[u_s \frac{\partial u_s}{\partial x_s} + v_s \frac{\partial u_s}{\partial y_s}\right] = 3 - \frac{\partial P}{\partial x_s} + \frac{\partial^2 u_s}{\partial y_s^2} \tag{2}$$

$$0 = -3\tan(\alpha+\beta) - \frac{\partial P}{\partial y_s} \tag{3}$$

where the subscript "s" denotes the variables in the slide region, and Reynolds number, Re, is defined to be

$$Re = \frac{\rho q}{\mu}, \tag{4}$$

where ρ is the liquid density, q is the flow rate per unit width, and μ is the liquid viscosity. The fully developed film thickness far upstream the slide, h_0, is the chosen unit of length and the average film speed of the fully developed flow, $\frac{q}{h_0}$, is the chosen characteristic velocity.

By using the appropriate boundary conditions at the solid surface and gas–liquid interface, and constant flow rate per unit width q, the velocity profile tangential to the slide is derived as follows:

$$u_s(x_s, y_s) = \frac{3}{h_s}\left[\frac{y_s}{h_s} - \frac{1}{2}\left(\frac{y_s}{h_s}\right)^2\right]. \tag{5}$$

The normal component of the velocity profile v_s is obtained from continuity equation (1), combined with no penetration condition at slide surface:

$$u_s(x_s, y_s) = u_s \frac{y_s}{h_s}\frac{dh_s}{dx_s}. \tag{6}$$

The pressure field is approximated by integrating the normal component of the momentum equation (3), and applying normal stress balance at the liquid–gas interface:

$$p = -\frac{1}{Ca}\frac{d\kappa_s}{dx_s} + 3(h_s - y_s)\tan(\alpha+\beta), \tag{7}$$

where the capillary number, Ca, is defined as

$$Ca = \frac{\mu q}{h_0 \sigma}, \tag{8}$$

σ is the liquid surface tension and κ is the curvature of the free surface, which for two-dimensional translationally symmetric meniscus is

$$\kappa = \frac{\frac{d^2h}{dx^2}}{\left[1 + \left(\frac{dh}{dx}\right)^2\right]^{\frac{3}{2}}}. \tag{9}$$

The film profile equation is obtained by inserting the approximate velocity profiles (5) and (6) together with the pressure profile (7) into the tangential component of the momentum Equation (2) and integrating it across the film thickness[1,5,6]:

$$\underbrace{\frac{1}{3Ca}\frac{d\kappa_s}{dx_s}}_{\text{Capillary Pressure Gradient}} = \underbrace{\frac{2}{5}Re\frac{1}{h_s^3}\frac{dh_s}{dx_s}}_{\text{Inertia}} + \underbrace{\tan(\alpha+\beta)\frac{dh_s}{dx_s}}_{\text{Cros-Streamwise Gravity}} + \underbrace{\frac{1}{h_s^3}}_{\text{Viscous}} - \underbrace{\frac{1}{1}}_{\text{Streamwise Gravity}} \tag{10}$$

Similar analysis can be constructed for the flow up the moving web. The corresponding film profile equation for the flow near the moving web is

$$\underbrace{\frac{1}{3Ca}\frac{d\kappa_w}{dx_w}}_{\text{Capillary Pressure Gradient}} = \left[\underbrace{\frac{Re}{15}\left(\frac{U_W^2}{h_w}-\frac{6}{h_w^3}\right)}_{\text{Inertia}} - \underbrace{\frac{\sin\beta}{\cos(\alpha+\beta)}}_{\text{Cross-Streamwise Gravity}}\right]\frac{dh_w}{dx_w} + \underbrace{\frac{1}{h_w^3}-\frac{U_W}{h_w^2}}_{\text{Viscous}} + \underbrace{\frac{\cos\beta}{\cos(\alpha+\beta)}}_{\text{Streamwise Gravity}}, \quad (11)$$

where U_W is the web speed measured in units of the average velocity of flow down far upstream the slide, $\frac{q}{h_0}$.

Asymptotic inflow and outflow boundary conditions

The film profile equations (10) and (11) are third-order nonlinear differential equations and therefore require three boundary conditions. Christodoulou and Scriven,[1] Nagashima,[5,6] and later Jung et al.[7] derived inflow and outflow boundary conditions from asymptotic solution of the equations, which are obtained by linearizing it upstream the slide and downstream the web where the flow is nearly fully developed. This derivation is summarized here. At a region far upstream of the slide, the deviation from the fully developed film thickness h_0 is small, and the dimensionless film thickness can be expressed as follows:

$$h_s(x_s) = 1 + \varepsilon_s h_s'(x_s), \quad (12)$$

where ε_s is a very small quantity. Similarly, at a region far downstream of the web, the dimensionless film thickness can be expressed as follows:

$$h_w(x_w) = \frac{h_\infty}{h_0} + \varepsilon_w h_w'(x_w). \quad (13)$$

where h_∞ is the fully developed thickness on the moving web. In this formulation, h_∞ cannot be specified independently of the web speed, U_W, to satisfy the imposed flow rate from the flow down the slide. Retaining terms through $o(\varepsilon_s)$ and $o(\varepsilon_w)$, the linearized film profile equations for slide and web flows are

$$\frac{d^2h_s'}{dx_s^3} - 3Ca\left[-\frac{2}{5}Re + \tan(\alpha+\beta)\right]\frac{dh_s'}{dx_s} + 9Cah_s' = 0, \quad (14)$$

and

$$\frac{d^3h_w'}{dx_w^3} + Ca\left\{\frac{Re}{5}\left[6\left(\frac{h_0}{h_\infty}\right)^3 - U_W^2\frac{h_0}{h_\infty}\right] + 3\frac{\sin\beta}{\cos(\alpha+\beta)}\right\}\frac{dh_w'}{dx_w} + 3Ca\left[3\left(\frac{h_0}{h_\infty}\right)^4 - 2U_W\left(\frac{h_0}{h_\infty}\right)^3\right]h_w' = 0. \quad (15)$$

Solutions of Eq. 14 have the general form

$$h_s'(x_s) = C_1e^{\lambda_{1,s}x_s} + C_2e^{\lambda_{2,s}x_s} + C_3e^{\lambda_{3,s}x_s} \quad (16)$$

where the λ_s are the roots of the characteristic polynomial

$$\lambda_s^3 - 3Ca\left[-\frac{2}{5}Re + \tan(\alpha+\beta)\right]\lambda_s + 9Ca = 0. \quad (17)$$

As Christodoulou and Scriven[1] and Nagashima[5,6] pointed out, of the three roots of Eq. 17, one is real and negative and the other two are complex conjugate roots with positive real part. This is true for slide inclination less than 20° measured from horizontal direction ($\alpha + \beta < 70°$), capillary number less than 1, and no inertia. At low capillary number, $Ca \leqq 0.01$, and creeping flow, $Re = 0$, this is always true for any slide inclination. Only roots with positive real part are physically relevant because the deviation from the fully developed film thickness should decay in the upstream direction. Consequently, only the complex roots are admissible. The solution of the linearized equation can be written in the following form:

$$h_s = 1 + \varepsilon_s \exp(\lambda_{r,s}x_s)\cos(\lambda_{i,s}x_s + \Phi) \quad (18)$$

where $\lambda_{r,s}$ represents the exponential decay constant, $\lambda_{i,s}$ represents the wavenumber of the standing wave, and Φ is the phase angle of the wave. A free parameter Robin-type boundary condition can be formed by a linear combination of Eq. 18 and its first and second derivatives to eliminate the parameters ε_s and Φ. This serves as the inflow boundary condition for the slide flow:

$$\frac{d^2h_s}{dx_s^2} - 2\lambda_{r,s}\frac{dh_s}{dx_s} + (\lambda_{r,s}^2 + \lambda_{i,s}^2)(h_s - 1) = 0 \quad \text{at } x_s = 0. \quad (19)$$

Similarly, the solutions of the linearized film profile equation for the flow up the moving web, Eq. 15, are of the following form:

$$h_w'(x_w) = C_1e^{\lambda_{1,w}x_w} + C_2e^{\lambda_{2,w}x_w} + C_3e^{\lambda_{3,w}x_w}, \quad (20)$$

where the λ_w are the three roots of the characteristic polynomial

$$\lambda_w^3 + Ca\left\{\frac{Re}{5}\left[6\left(\frac{h_0}{h_\infty}\right)^3 - U_W^2\frac{h_0}{h_\infty}\right] + 3\frac{\sin\beta}{\cos(\alpha+\beta)}\right\}\lambda_w + 3Ca\left[3\left(\frac{h_0}{h_\infty}\right)^4 - 2U_W\left(\frac{h_0}{h_\infty}\right)^3\right] = 0. \quad (21)$$

In the web region, the deviation from the fully developed film thickness should decay along the downstream direction. Consequently, only the real negative root of the characteristic polynomial is admissible. The solution is

$$h_w = \frac{h_\infty}{h_0} + \varepsilon_w \exp(\lambda_{r,w}x_w). \quad (22)$$

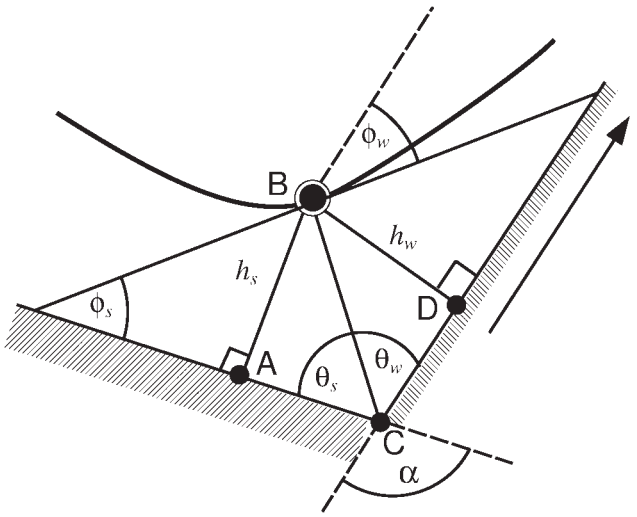

Figure 3. Matching the flows.

Two linearly independent Robin-type asymptotic outflow boundary conditions can be derived from Eq. 22:

$$\frac{dh_{\mathrm{w}}}{dx_{\mathrm{w}}} - \lambda_{\mathrm{r,w}}\left(h_{\mathrm{w}} - \frac{h_\infty}{h_0}\right) = 0 \quad \text{at } x_{\mathrm{w}} = L_{\mathrm{W}}; \tag{23}$$

$$\frac{d^2h_{\mathrm{w}}}{dx_{\mathrm{w}}^2} - \lambda_{\mathrm{r,w}}^2\left(h_{\mathrm{w}} - \frac{h_\infty}{h_0}\right) = 0 \quad \text{at } x_{\mathrm{w}} = L_{\mathrm{W}}. \tag{24}$$

Because these inflow and outflow boundary conditions are independent from the departure measure of fully developed thickness, ε_{s} and ε_{w}, and phase angle, Φ, that depends on the location of the boundary, they can be applied at any location, providing that the linearized film profile equations are still valid there.

Matching conditions

The matching between the flow down the slide and up the moving web is done by requiring the film thickness, its slope, and its curvature to be continuous at an arbitrarily chosen matching point. These matching conditions serve as two outflow boundary conditions for the slide flow and one inflow boundary condition for the web flow, thus completing the boundary condition set of each flow region.

Film thickness matching is shown in Figure 3. Triangle ABC and BCD have a common hypotenuse at line BC. From the trigonometric law of sines, the film thickness of the slide flow, h_{s}, and that of the web flow, h_{w}, are related by

$$\frac{h_{\mathrm{s}}}{\sin\,\theta_{\mathrm{s}}} = \frac{h_{\mathrm{w}}}{\sin\,\theta_{\mathrm{w}}}. \tag{25}$$

Nagashima[5,6] chose to set the matching location on the bisector ray of the angle between the slide and the web, such that $\theta_{\mathrm{s}} = \theta_{\mathrm{w}}$, and the thickness matching condition reduces to equal film thickness, i.e., $h_{\mathrm{s}} = h_{\mathrm{w}}$. We also used equal-angle bisecting ray as the matching point in most of our calculations. However, as explained later in section "Effect of Matching Location", we also used other bisecting angle as well and investigated its effect to the computed thickness profile.

Matching slope of the two profiles is equivalent to relate their inclinations, $\phi_{\mathrm{s}} \equiv \tan^{-1}\left(\frac{dh_{\mathrm{s}}}{dx_{\mathrm{s}}}\right)$ and $\phi_{\mathrm{w}} \equiv \tan^{-1}\left(\frac{dh_{\mathrm{w}}}{dx_{\mathrm{w}}}\right)$, as depicted in Figure 3. Mathematically, ϕ_{s} and ϕ_{w} are related by

$$\phi_{\mathrm{w}} = \phi_{\mathrm{s}} + \alpha - \pi \tag{26}$$

Curvature of a profile is independent of its orientation in space and therefore independent from the coordinate system. The curvature matching condition is simply

$$\kappa_{\mathrm{s}} = \kappa_{\mathrm{w}} \tag{27}$$

Transformation to arc-length coordinate

To improve the performance of the numerical method used to solve the film profile equations, the equations are recast in an arc length coordinate system defined along the free surface. This approach was not used by Nagashima[5,6] and Jung et al.[7] although Kheshgi et al.[9] had reported great success of using arc length coordinate to solve the film profile equations. The advantage of the arc length coordinates is that it is, by definition, monotonic along the free surface and so avoids the singularities caused by meniscus inclination of 90° or even double valued film thickness profile when they are expressed in Cartesian coordinates. Such cases would guarantee failure for any numerical method used for solving them, unless the coordinate system is locally switched to eliminate the singularities, which is impractical. The third-order ODE written in terms of Cartesian coordinates along the slide and web that describe the film profile equations are transformed into a system of three first-order ODE written in terms of the arc length coordinate plus one additional ODE that relates both coordinate systems. At the slide region, the ODE system is

$$\frac{dh_{\mathrm{s}}}{ds} = \sin\,\phi_{\mathrm{s}}, \tag{28}$$

$$\frac{d\phi_{\mathrm{s}}}{ds} = \kappa_{\mathrm{s}}, \tag{29}$$

$$\frac{1}{3Ca}\frac{d\kappa_{\mathrm{s}}}{ds} = \left[-\frac{2}{5}Re\,\frac{1}{h_{\mathrm{s}}^3} + \tan(\alpha+\beta)\right]\sin\phi_{\mathrm{s}} + \left[\frac{1}{h_{\mathrm{s}}^3} - 1\right]\cos\,\phi_{\mathrm{s}}, \tag{30}$$

$$\frac{dx_{\mathrm{s}}}{ds} = \cos\,\phi_{\mathrm{s}}. \tag{31}$$

At the web region, the ODE system is

$$\frac{dh_{\mathrm{w}}}{ds} = \sin\,\phi_{\mathrm{w}}, \tag{32}$$

$$\frac{d\phi_{\mathrm{w}}}{ds} = \kappa_{\mathrm{w}}, \tag{33}$$

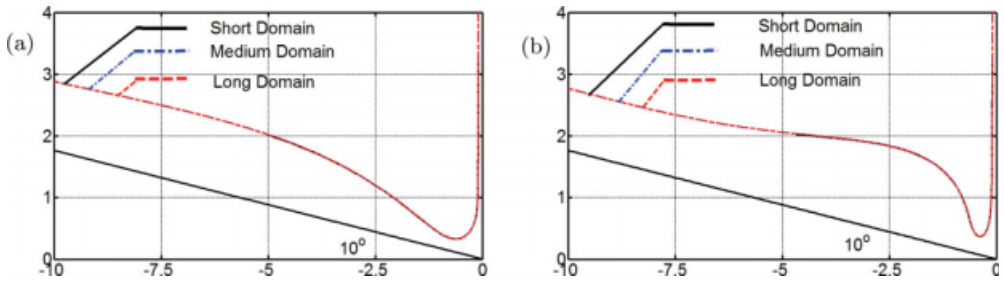

Figure 4. Effect of domain length.

(a) $Ca = 0.01$, $Re = 0$; (b) $Ca = 0.1$, $Re = 10$. $\alpha = 80°$, $\beta = 0°$, $U_W = 10$. $\alpha = 80°$, $\beta = 0°$, $U_W = 10$. [Color figure can be viewed in the online issue, which is available at www.interscience.wiley.com.]

$$\frac{1}{3Ca}\frac{d\kappa_w}{ds} = \left[\frac{Re}{15}\left(\frac{U_W^2}{h_w} - \frac{6}{h_w^3}\right) - \frac{\sin\beta}{\cos(\alpha+\beta)}\right]\sin\phi_w + \left[\frac{1}{h_w^3} - \frac{U_W}{h_w^2} + \frac{\cos\beta}{\cos(\alpha+|\beta)}\right]\cos\phi_w,$$

$$\frac{dx_w}{ds} = \cos\phi_w. \tag{35}$$

The inflow and outflow boundary conditions in arc-length coordinates are

$$\frac{\kappa_s}{\cos\phi_s} - 2\lambda_{r,s}\tan\phi_s + \left(\lambda_{r,s}^2 + \lambda_{i,s}^2\right)(h_s - 1) = 0 \tag{36}$$

at slide inflow

$$\tan\phi_w - \lambda_{r,w}\left(h_w - \frac{h_\infty}{h_0}\right) = 0 \quad \text{at web outflow} \tag{37}$$

$$\frac{\kappa_w}{\cos\phi_w} - \lambda_{r,w}^2\left(h_w - \frac{h_\infty}{h_0}\right) = 0 \quad \text{at web outflow} \tag{38}$$

In addition to these boundary conditions, three matching conditions, Eq. 25–27 are also imposed at the slide outflow and web inflow to close the system.

Solution method

Both film profile equations written in terms of arc-length coordinates take the form of a system of four coupled first-order ODE, one of which is nonlinear. The system was discretized by a second-order (centered difference stencil) finite difference method. The resulting nonlinear algebraic system of equation was solved by Newton's method.

The mesh was graded in the highly curved region, i.e., at the vicinity of matching region, to capture the steep gradient in thickness profile and to reduce computation effort. The mesh was graded with appropriate one-dimensional stretching functions compiled by Vinokur[10] and de Santos.[11]

At the slide region, the nodes are concentrated at the matching point, i.e., $\xi_s = N_s$, and the stretching function used is

$$s\left(\frac{\xi_s}{N_s}\right) = \frac{\tanh\left(A_s\frac{\xi_s}{N_s}\right)}{\tanh A_s} \tag{39}$$

where A_s represents the strength of node concentration at $\xi_s = N_s$. If the spacing at $\xi_s = N_s$ is specified (ΔS_{N_s}), A_s must satisfy

$$\sinh 2A = \frac{2A}{N\Delta S_{N_s}}. \tag{40}$$

Similarly, the nodes at the web region are concentrated at the matching point, i.e., $\xi_w = 0$, and the stretching function used is

$$s\left(\frac{\xi_w}{N_w}\right) = 1 + \frac{\tanh\left[A_w\left(\frac{\xi_w}{N_w} - 1\right)\right]}{\tanh A_w} \tag{41}$$

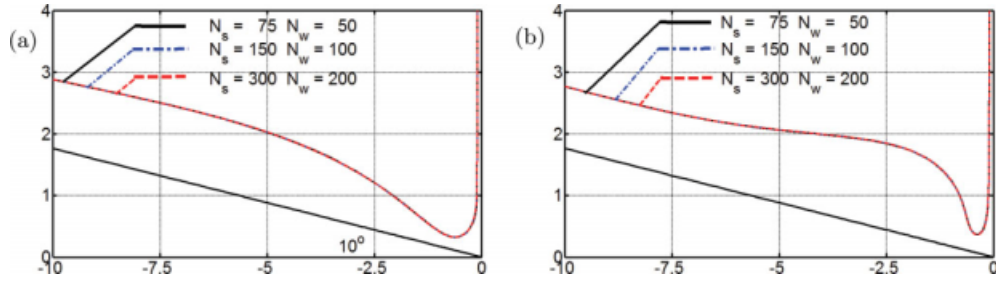

Figure 5. Effect of number of nodes.

(a) $Ca = 0.01$, $Re = 0$; (b) $Ca = 0.1$, $Re = 10$. $\alpha = 80°$, $\beta = 0°$, $U_W = 10$. [Color figure can be viewed in the online issue, which is available at www.interscience.wiley.com.]

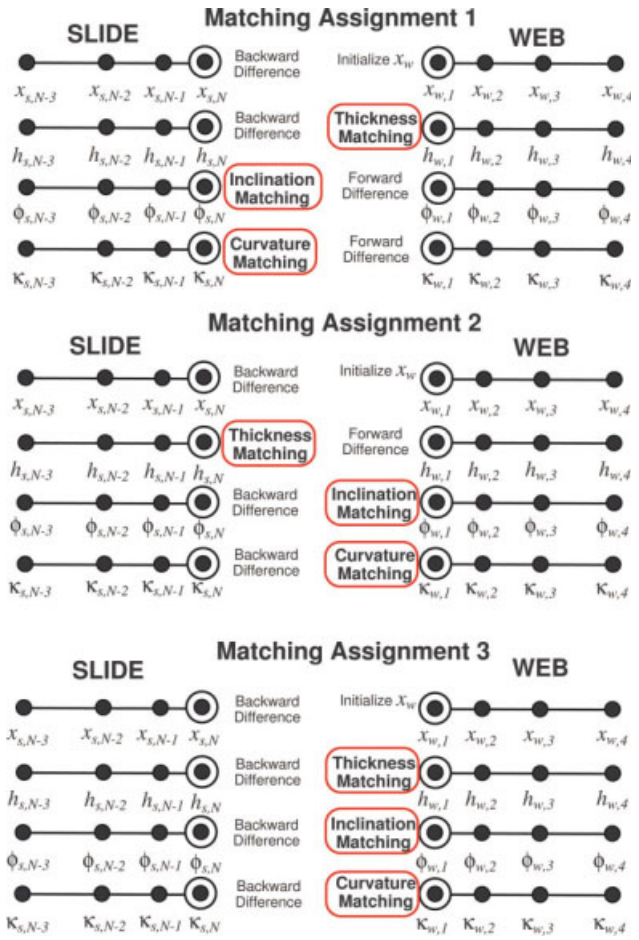

Figure 6. Ways of assigning matching conditions I.

[Color figure can be viewed in the online issue, which is available at www.interscience.wiley.com.]

where A_w represents the strength of node concentration at $\xi_w = 0$. If the spacing at $\xi_w = 0$ is specified (ΔS_0), A_w must satisfy

$$\sinh 2A_w = \frac{2A_w}{N_w \Delta S_0}. \tag{42}$$

The domain lengths were set at $15h_0$ and $5h_0$ for slide and web regions, respectively. The numbers of nodes deployed were 150 and 100 for slide and web regions, respectively. The effect of these arbitrary choices of domain lengths on the solution is discussed in the following section.

Results

Effect of domain length

Imposing inflow and outflow boundary conditions as Robin boundary conditions permits the domain of calculation to be shorter than when Dirichlet and Neumann boundary conditions are imposed and the level of accuracy of the approximation is fixed.[12] However, the domain length chosen has to be long enough such that the computed solution is insensitive to the arbitrary location of the synthetic flow boundaries. In this study, the sensitivity of the slide and web domain lengths, parameterized as a total arc length along the free surface, S_S and S_W, was tested on slide–web inclination and flow parameter sets that are representative of actual coating operations. The slide and web inclinations were set at 10° and 90° horizontally, as depicted in Figure 4. The sensitivity analysis was done at two cases, low capillary number with zero inertia, $Ca = 0.01$ and $Re = 0$, and moderate capillary and Reynolds numbers, $Ca = 0.1$ and $Re = 10$. The three domain lengths tested were:

- Short: $S_S = 5h_0$; $S_W = 3h_0$
- Medium: $S_S = 15h_0$; $S_W = 5h_0$
- Long: $S_S = 30h_0$; $S_W = 10h_0$

Nodes were distributed uniformly along the free surface of the domain, 20 nodes per unit arc-length along the slide and web, so that the distribution was invariant as the domain length was changed. The computed film thickness profiles with each domain length are presented in Figure 4.

The solutions are virtually the same for the cases tested, even for the case of flow with inertia and higher capillary number, which is expected to require longer domain length due to the presence of a standing wave near the matching point. The domain length chosen for the analysis

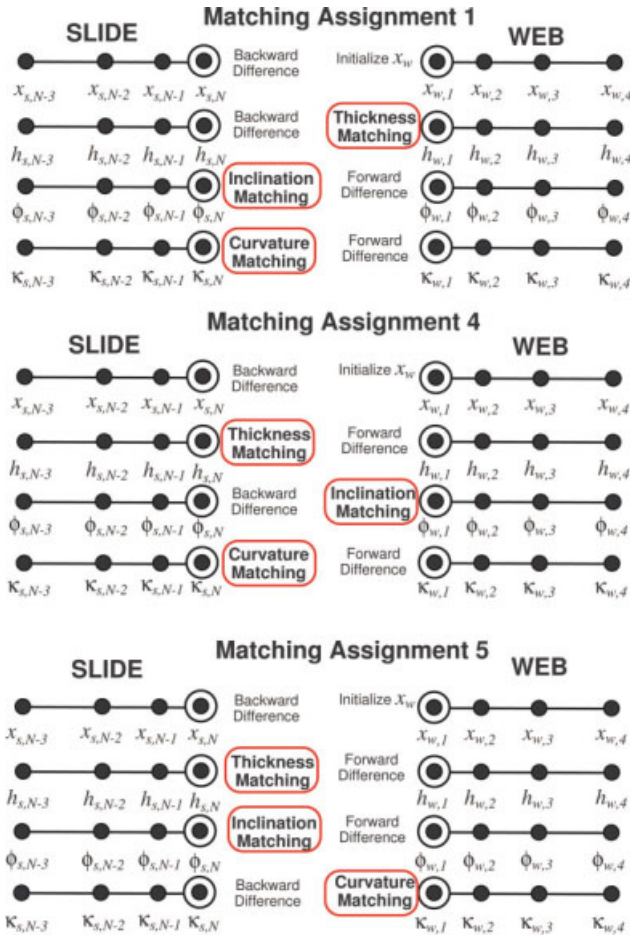

Figure 7. Ways of assigning matching conditions II.

[Color figure can be viewed in the online issue, which is available at www.interscience.wiley.com.]

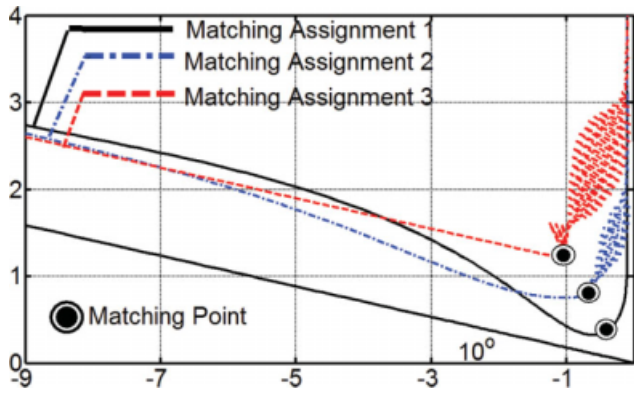

Figure 8. Effect of matching conditions assignment I.

$\alpha = 80°$, $\beta = 0°$, $Ca = 0.01$, $Re = 0$, $U_W = 10$. [Color figure can be viewed in the online issue, which is available at www.interscience.wiley.com.]

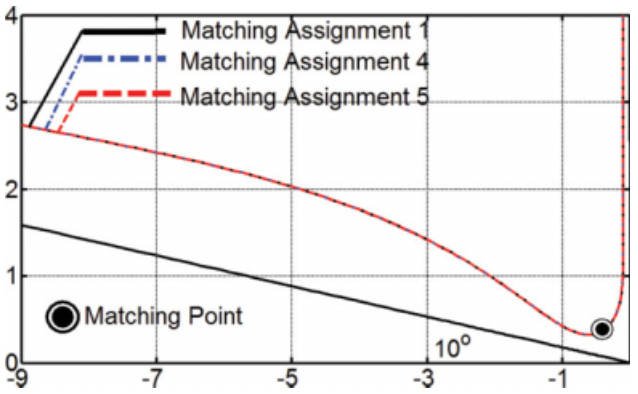

Figure 9. Effect of matching conditions assignment II.

$\alpha = 80°$, $\beta = 0°$, $Ca = 0.01$, $Re = 0$, $U_W = 10$. [Color figure can be viewed in the online issue, which is available at www.interscience.wiley.com.]

presented from now on was slide domain of 15 h_0 and web domain of 5 h_0.

Effect of mesh

The sensitivity of the solution to the level of discretization, i.e., the numbers of nodes used, was tested at the same parameters used to test the effect of domain length, i.e., $Ca = 0.01$ and $Re = 0$, and, $Ca = 0.1$ and $Re = 10$. The analysis was done for three different number of nodes for the slide flow N_s and the web flow N_w:

- $N_s = 75$ and $N_w = 50$
- $N_s = 150$ and $N_w = 100$
- $N_s = 300$ and $N_w = 200$

The computed thickness profiles are presented in Figure 5. The solutions are insensitive to the mesh at both set of parameters. The results presented from now on were obtained using $N_s = 150$ and $N_w = 100$.

Effect of matching conditions assignments

To impose boundary and matching conditions in the finite difference approximation of the film profile equations, some of the residual equations that come from the discretized ODE at the nodes located at inflow, outflow, and matching points have to be replaced by boundary and matching conditions. Matching the thickness, slope, and curvature requires three conditions that can be assigned to replace three out of six finite difference equations at the matching nodes of a combined slide and web domains, and there are several ways to do that.

To test the sensitivity of the solutions to the different ways of imposing matching conditions, we performed numerical experiment on a base case: $Ca = 0.01$, $Re = 0$, $U_W = 10$, at slide-web folding angle $\alpha = 80°$ and web angle $\beta = 0°$. The nodes are concentrated near the matching point with appropriate stretching functions as mentioned in section "Solution Method". Five matching conditions assignments were tested, and their illustrations are presented in Figure 6 and 7. The first set is as follows:

- Matching Assignment 1: Inclination and curvature matching conditions, Eq. 26 and 27, are imposed in the matching node of the slide flow domain by replacing finite difference approximations of Eq. 29 and 30 (ODEs for the free surface inclination and curvature), respectively. Thickness matching condition, Eq. 25, is imposed in the matching node of the web flow domain by replacing the finite difference approximation of Eq. 32 (ODE for the film thickness).
- Matching Assignment 2: Thickness matching condition, Eq. 25, is imposed in the matching node of the slide flow domain by replacing the finite difference approximations of Eq. 28 (ODE for the film thickness). Inclination and

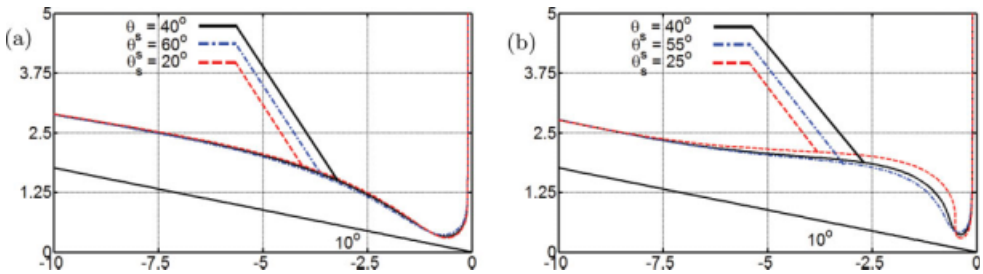

Figure 10. Effect of matching location.

(a) $Ca = 0.01$, $Re = 0$; (b) $Ca = 0.1$, $Re = 10$. $\alpha = 80°$ $\beta = 0°$, $U_W = 10$. [Color figure can be viewed in the online issue, which is available at www.interscience.wiley.com.]

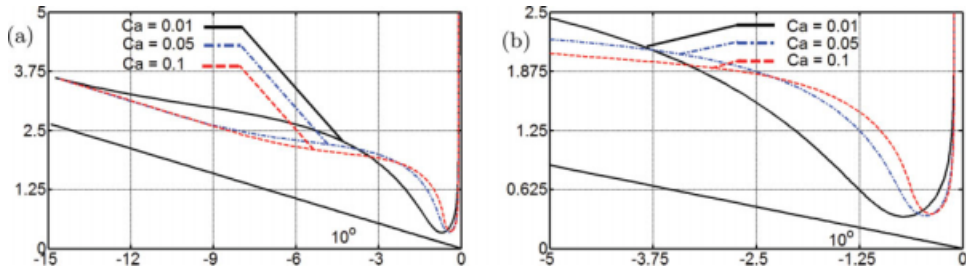

Figure 11. Effect of capillary number.

(a) Overall profile; (b) Bead region. $\alpha = 80°$, $\beta = 0°$, $Re = 10$ $U_W = 10$. [Color figure can be viewed in the online issue, which is available at www.interscience.wiley.com.]

curvature matching conditions, Eq. 26 and 27, are imposed in the first node of the web domain by replacing finite difference approximations of Eq. 33 and 34 respectively (ODEs for the free surface inclination and curvature). This is the opposite of the Matching Assignment 1.

- Matching Assignment 3: All matching conditions, i.e., Eq. 25–27), are assigned by replacing the finite difference approximations of Eq. 32–34 in the matching node of the web region.

The computed thickness profiles with each one of the matching condition assignments are shown in Figure 8. The film profiles obtained with Matching Assignments 2 and 3 present oscillations in the web flow region only. Moreover, wiggles from Matching Assignment 3 have greater amplitudes and are damped at a distance further downstream than the wiggles from Matching Assignment 2. The oscillations arise because the system of equations for the web flow alone becomes overspecified while using more than one matching condition. Moreover, the wiggles become more severe as the equation system is further constrained, as it happens with Matching Assignment 3. The film profile equation of the web flow is a third-order ODE and it already has two outflow boundary conditions, Eq. 23 and 24. To make the system well posed, only one additional condition is needed and that is provided by one matching condition. Imposing more than one matching condition, in addition to the already specified two outflow boundary condition, will be analogous to imposing more than three boundary conditions to a third-order ODE and the system becomes overspecified. The excessive constraints then produce an oscillatory solution, as shown in Figure 8, to satisfy all of the imposed conditions at the domain boundaries.

Nevertheless, Matching Assignment 1 is not a unique working combination. A second set of matching condition assignments, illustrated in Figure 7, were tested and the computed thickness profiles are shown in Figure 9. Matching Assignments 4 and 5, depicted in Figure 7, just as in Matching condition 1, two matching conditions are imposed on the slide flow and one matching condition is imposed on the web flow. What differs is the differential equations that is sacrificed and what matching condition is used. All assignment schemes shown in Figure 7 do not overspecify the equation system on the slide nor the web. As expected, they all yielded solutions without oscillations.

The main conclusion is that although the system of equations for the slide and web flows are solved simultaneously, it is not enough to satisfy the number of boundary and matching conditions globally. Each set of ODE that describes the flow down the slide and up the web should have the appropriate number of boundary conditions.

Effect of matching location

As described, viscocapillary model of slide coating consists of a model of the flow down the slide and a model of the flow up the web spliced at a chosen matching point by matching conditions. The location of the matching point is arbitrary and it is defined in terms of the angle θ_s specified in the thickness matching condition, Eq. 25. As the angle θ_s falls, the matching location is shifted further upstream the slide. This may have a strong effect on the predicted film thickness profile.

Nagashima[5,6] set the matching point to be along the bisector line, where $\theta_s = \frac{\alpha}{2}$, and never investigated the effects of changing the matching point location on the computed thickness profile. We explored this by comparing predictions at

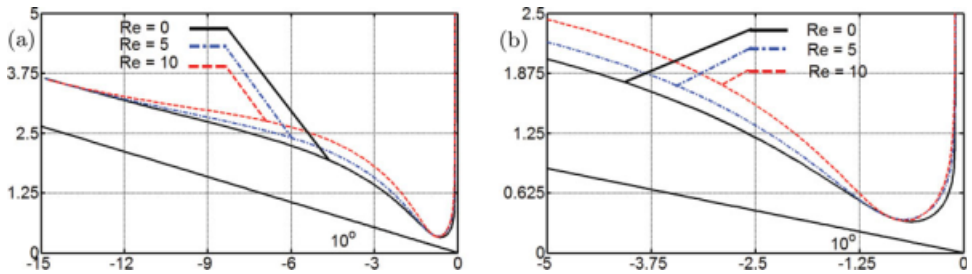

Figure 12. Effect of Reynolds number.

(a) Overall profile; (b) Bead region. $\alpha = 80°$, $\beta = 0°$, $Ca = 0.01$, $U_W = 10$. [Color figure can be viewed in the online issue, which is available at www.interscience.wiley.com.]

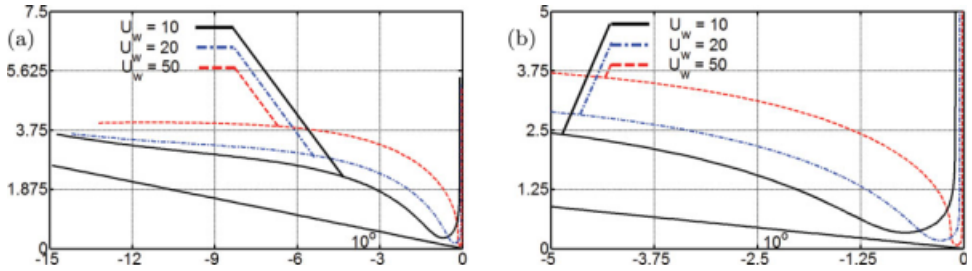

Figure 13. Effect of web speed.

(a) Overall profile; (b) Bead region. $\alpha = 80°$, $\beta = 0°$, $Ca = 0.01$, $Re = 10$. [Color figure can be viewed in the online issue, which is available at www.interscience.wiley.com.]

different values of θ_s. The computed thickness profiles are presented in Figure 10.

At low capillary number and vanishing Reynolds number, the effect of the matching point location is weak. The gradient of the curvature of the film profile is small and each term of the film profile equation does not change much as the matching point is translated up or downstream. At higher capillary and Reynolds numbers, the meniscus is highly curved and the curvature gradient is also high near the matching point. Therefore, changes on the location of the matching point is accompanied by large changes in the magnitude of each term of both film profile equations. The prediction then becomes very sensitive to the location of the matching point, as shown in Figure 10b. The effect is more pronounced on the film profile on the slide where a standing wave is formed. Which solution is more accurate can be determined only by comparing all the three profiles with the solution of the complete two-dimensional Navier-Stokes equation.

Effect of operating conditions

What follows is an analysis on how different operating conditions affect the film profile along the slide and web. Changes in free surface configuration may explain important operating limits of slide coating process. For all cases examined here, the matching condition assignment used is what was referred as Matching Assignment 1 in section "Effect of Matching Conditions Assignments" with the matching location at the bisecting ray between the slide and the web. The parameters that govern the slide coating flow are the capillary number $Ca = \frac{\mu q}{\sigma h_0}$, the Reynolds number $Re = \frac{\rho q}{\mu}$, dimensionless web speed $U_W = \frac{V_{web} h_0}{q}$, and parameters that define the flow geometry.

The evolution of the film profile over the slide and web as the capillary number changes is presented in Figure 11 at Reynolds number $Re = 10$, dimensionless web speed $U_W = 10$, web inclination with respect to vertical $\beta = 0°$, and the inclination between slide and web $\alpha = 80°$. As the capillary number rises, the meniscus near the turnaround region becomes more curved to keep the low pressure under the free surface. This low pressure creates an adverse pressure gradient along the web that counteracts the drag of the upward moving web. The thinner the deposited layer, the higher needs to be the adverse pressure gradient. The capillary number also has a strong effect on the configuration of the standing wave formed on the foot of the slide. Its

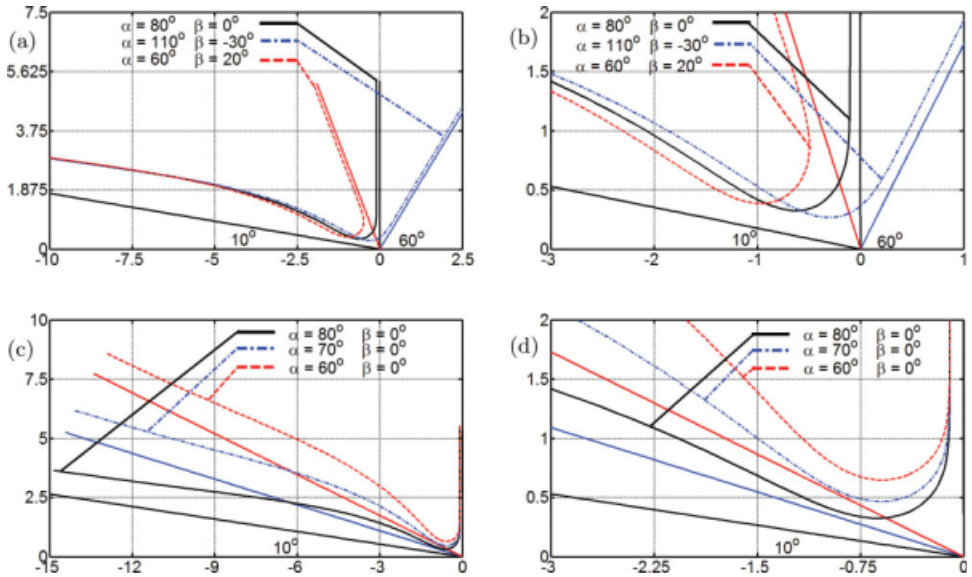

Figure 14. Effect of web inclination.

Effect of web inclination: (a) Overall profile and (b) bead region. Effect of slide inclination: (c) overall profile and (d) bead region. $Ca = 0.01$, $Re = 0$, $U_W = 10$. [Color figure can be viewed in the online issue, which is available at www.interscience.wiley.com.]

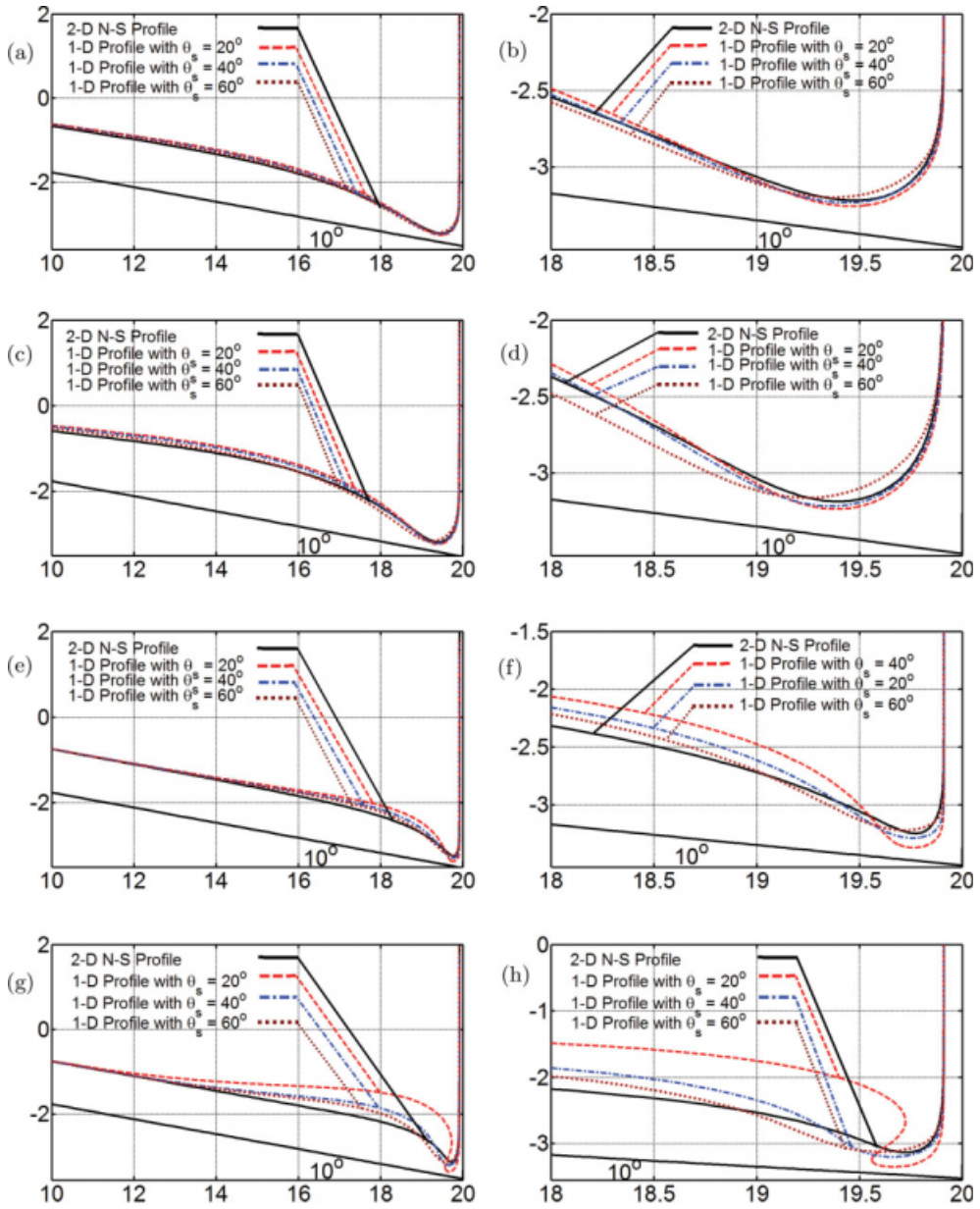

Figure 15. Comparison with 2D N-S profile at different capillary and Reynolds numbers.

(a) $Ca = 0.009$, $Re = 0.3$, overall profile; (b) $Ca = 0.009$, $Re = 0.3$, bead region; (c) $Ca = 0.009$, $Re = 7$, overall profile; (d) $Ca = 0.009$, $Re = 7$, bead Region; (e) $Ca = 0.09$, $Re = 0.3$, overall profile; (f) $Ca = 0.09$, $Re = 0.3$, bead region; (g) $Ca = 0.09$, $Re = 7$, overall profile; (h) $Ca = 0.09$, $Re = 7$, bead region. $\alpha = 80°$, $\beta = 0°$, $U_W = 11$. [Color figure can be viewed in the online issue, which is available at www.interscience.wiley.com.]

wavelength increases as the capillary force becomes stronger, i.e., lower capillary number. Consequently, the departure of the film profile from its fully developed value decays slower along the upstream direction.

The effect of Reynolds number, in a range from 0 to 10, at capillary number $Ca = 0.01$ is shown in Figure 12. The effect on the free surface curvature near the matching point is small. However, as the Reynolds number rises, the adverse pressure gradient necessary to slow down the flow down the slide increases to compete with the higher inertial force. Consequently, the amplitude of the standing wave near the bottom of the slide becomes larger.

The thickness of the coated layer falls as the dimensionless web speed rises at a constant Reynolds and capillary numbers. Therefore, a stronger adverse pressure gradient along the web is needed to measure the liquid dragged by the moving web. The adverse pressure gradient is created by a lower pressure under the meniscus that becomes more curved as thickness falls, as shown in Figure 13. The thickness of the liquid film under the meniscus also falls, and therefore a higher pressure upstream of the turnaround flow region is needed to keep the flow rate constant. This explains the high amplitude standing wave on the foot of the slide observed at high U_W. The small radius of curvature of the

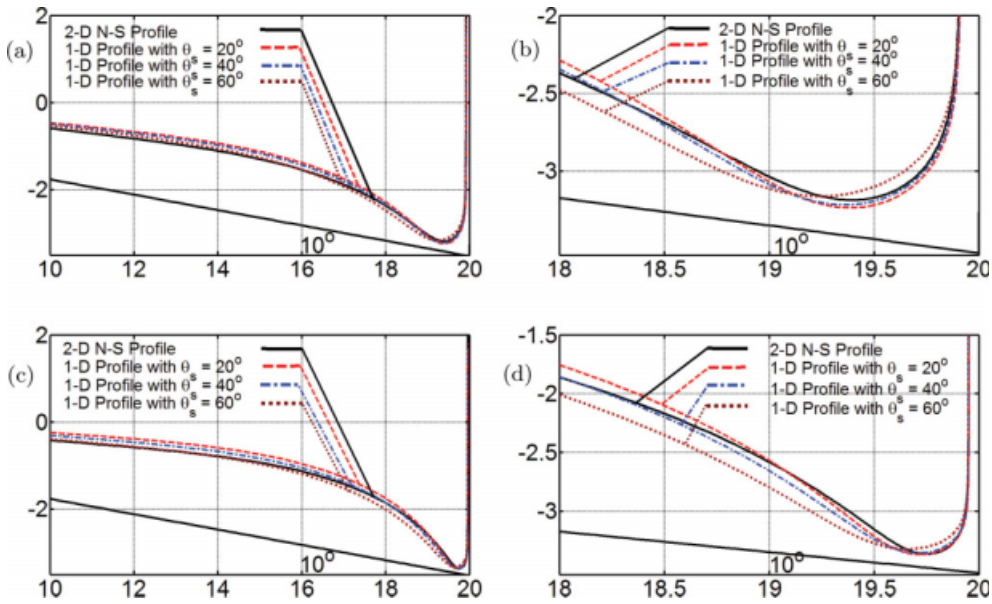

Figure 16. Comparison with 2D N-S profile at different web speed.

(a) $U_w = 11$ overall profile; (b) $U_w = 11$, bead region; (c) $U_w = 20$, overall profile; (d) $U_w = 20$, bead region. $\alpha = 80°$, $\beta = 0°$, $Ca = 0.009$, $Re = 7$. [Color figure can be viewed in the online issue, which is available at www.interscience.wiley.com.]

meniscus combined with the large amplitude standing wave may lead to an unstable film profile that would define the maximum dimensionless web speed for stable flow.

The effect of slide and web inclination is shown in Figure 14. As the folding angle between slide and web α decreases, the liquid has to make sharper turn, from parallel to the slide surface to parallel to the web surface. The sharp change of the flow direction and the geometric restriction on the meniscus configuration lead to smaller radius of curvature of the free surface near the matching point. The stronger adverse pressure gradient along the web may lead to unstable flow that define the smallest slide—web inclination for stable operation.

Validation of the Asymptotic Model: Comparison with Solution of the 2D Navier-Stokes

The range of validity of the nonlinear asymptotic model was tested by comparing its prediction of free surface profile with the solution of the full 2D Navier-Stokes system with the appropriate boundary conditions to account for the free surface.

Because of the free surfaces, the flow domain at each parameter is unknown a priori. To solve this free boundary problem by means of standard techniques for boundary-value problems, the set of differential equations and boundary conditions posed in the unknown physical domain is transformed into an equivalent set defined in a known reference domain. This transformation is made by a mapping that connects both domains.

The Navier-Stokes system and the mapping (mesh generation) equations were solved all together by the Galerkin finite-element method. Biquadratic basis functions were used to represent both the velocity and the mapping from the reference to the physical domain. The basis functions used to represent the pressure field were piecewise, linear, and discontinuous. Once all the variables are represented in terms of the basis functions, the system of partial differential equations reduces to simultaneous algebraic equations for the coefficients of the basis functions of all the fields. This set of equations is nonlinear and sparse. It was solved by Newton's method. The linear system of equations at each Newtonian iteration was solved using a frontal solver.

The details of the formulation and solution method are not presented here, but they are similar to the ones used to study the slot coating process[13] and based on the pioneering work of Christodoulou and Scriven[1] and de Santos.[11]

Because the viscocapillary model neglects the presence of the upstream meniscus of slide coating flow, the comparison only entails the prediction of the top free surface profile. The goal of the comparison was also to determine the appropriate matching point location that connects the slide and web flows. Three different matching locations were used in most of the comparisons presented here.

The solutions obtained with the 1D viscocapillary model were compared with the full 2D Navier-Stokes predictions at different capillary and Reynolds numbers for three different matching locations. The 2D solutions were obtained with coating gap of 300 μm. At low Reynolds and capillary numbers, $Re = 0.3$ and $Ca = 0.009$, Figure 15ab, the film thickness profile predicted by both models are similar. As discussed before, at this set of parameters, the curvature of the free surface in the turnaround region is small, making the solution almost insensitive to the matching point location. Moreover, all terms of the film profile equations are small near the matching point, making the viscocapillary model accurate. The matching location at $\theta_s = 40°$ yielded the prediction closest to the full 2D solutions of the flow. At higher Reynolds number, $Re = 7$, and same capillary number, $Ca = 0.009$, Figure 15c,d, the agreement near the matching is

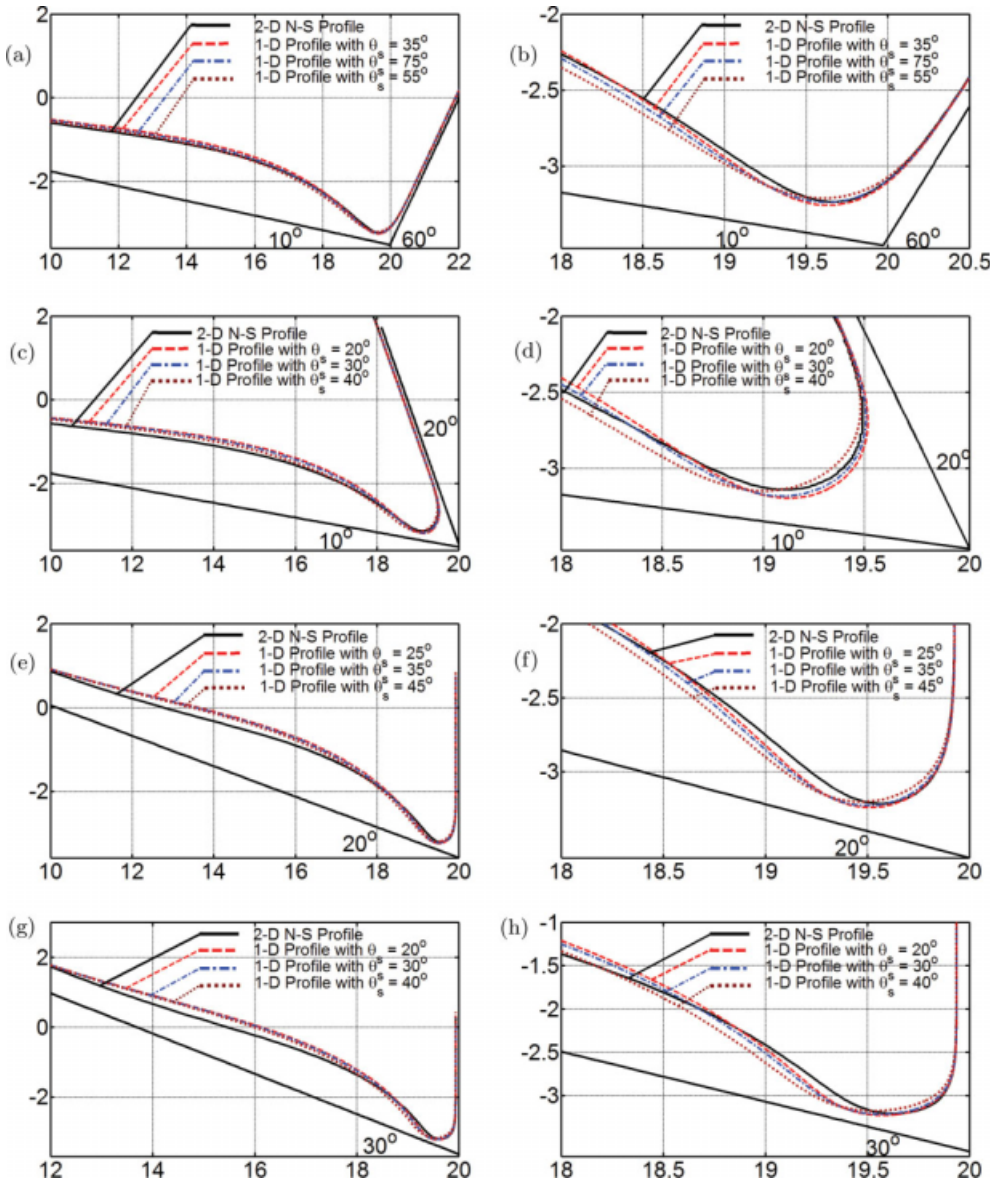

Figure 17. Comparison with 2D N-S profile at different slide—web inclinations.

(a) $\alpha = 100°$, $\beta = -30°$, overall profile; (b) $\alpha = 100°$, $\beta = -30°$, bead region; (c) $\alpha = 60°$, $\beta = 20°$, overall profile; (d) $\alpha = 60°$, $\beta = 20°$, bead region; (e) $\alpha = 70°$, $\beta = 0°$, overall profile; (f) $\alpha = 70°$, $\beta = 0°$, bead region; (g) $\alpha = 60°$, $\beta = 0°$, overall profile; (h) $\alpha = 60°$, $\beta = 0°$, bead region. $Ca = 0.009$, $Re = 7$, $U_W = 11$. [Color figure can be viewed in the online issue, which is available at www.interscience.wiley.com.]

still good, except the profile obtained with $\theta_s = 60°$. At higher capillary number, $Ca = 0.09$, Figure 15eh, the discrepancy between the computed film thickness profile is large. In this range, predictions obtained with $\theta_s = 60°$ were the ones closest to the full 2D solutions. An inappropriate choice of matching point location can lead to highly inaccurate free surface shape, as shown in Figure 15h. At higher capillary number, locating the matching point toward the web flow and extending the slide flow film profile solution further downstream improves the accuracy of the viscocapillary model.

Figure 16 shows the comparison between 1D and 2D predictions at low capillary number, $Ca = 0.009$, and $Re = 7$, at different web speeds U_W. As it rises, the film thickness deposited on the web falls and a stronger adverse pressure gradient is needed measure the flow up the moving web. The 1D viscocapillary model is able to capture this behavior and the agreement with the predictions from 2D model is good in the parameter range explored. The smallest relative error was obtained when the matching point location was $\theta_s = 40°$.

The effect of the slide and web inclinations on the accuracy of the viscocapillary model is shown in Figure 17. The comparison was done at $Ca = 0.009$, $Re = 7$, and $U_W = 11$. The agreement is satisfactory over the range of inclinations explored. It is clear, however, that the accuracy of the 1D

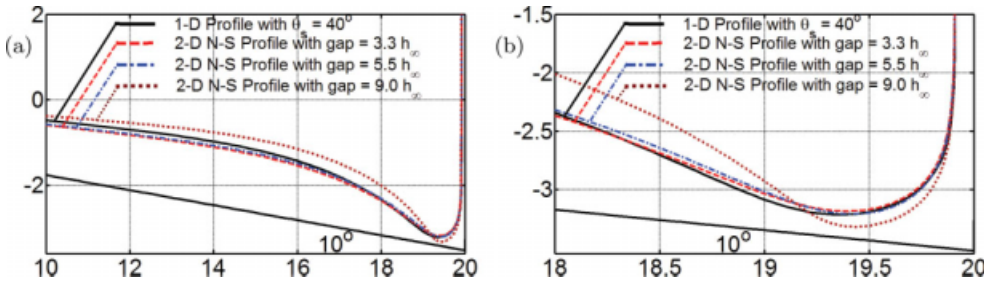

Figure 18. Comparison with 2D N-S Profile at different gaps.

(a) Overall profile; (b) Bead region. $\alpha = 80°$, $\beta = 0°$, $Ca = 0.009$, $Re = 7$, $U_W = 11$. [Color figure can be viewed in the online issue, which is available at www.interscience.wiley.com.]

model improves as the angle between the slide and the web rises. At larger angles, as presented in Fig. 17a,b, the radius of curvature of the meniscus is large, and consequently subambient pressure under the meniscus is low, leading to the smaller pressure gradient down the slide and up the web.

The comparison between the 1D viscocapillary model's prediction and 2D Navier-Stokes theory's was also performed at different slide–web gap to check the range at which the 1D model, which does not take the gap into account, is valid. Because of the lack of gap as a parameter in the viscocapillary model and to make a fair comparison, the computed thickness profiles from 2D Navier-Stokes theory at different gaps were translated along the slide surface such that the thickness profile on the web overlap one another. Figure 18 shows the free surface profile obtained with the viscocapillary model and with the full 2D Navier-Stokes model at there different gaps, covering the range from $3.3h_\infty$ to $9.0h_\infty$ at $Ca = 0.009$, $Re = 7$, and $U_W = 11$. If the gap is small enough, the 2D solution is virtually insensitive to this parameter, and the 1D predictions agree with the full 2D Navier-Stokes solutions. At larger gaps, the coating bead can no longer be treated as a liquid pool and the meniscus tends to curve toward the gap. In this case, the 1D predictions are not accurate and the viscocapillary model is not valid. This result shows that the use of viscocapillary model should be limited to cases at which the gap-to-thickness ratio is less than approximately 6.0.

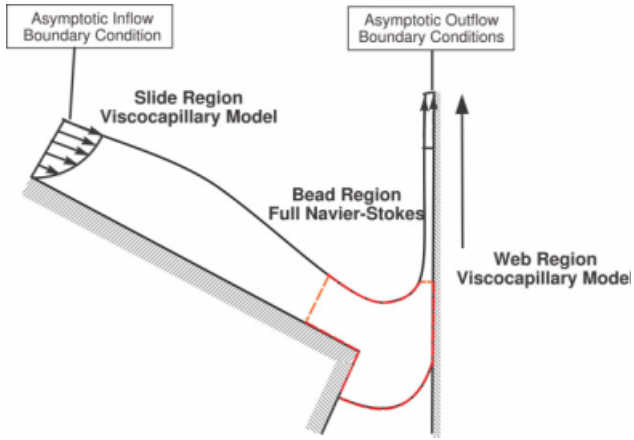

Figure 19. Proposed 1D 2D hybrid model.

[Color figure can be viewed in the online issue, which is available at www.interscience.wiley.com.]

Conclusions

In this article, a critical review of the available viscocapillary model is presented. We improve on the more accurate available model by writing it in terms of an arc-length coordinate along the free surface and by making the matching location adjustable. We have demonstrated that with the appropriate formulation, a simplified 1D viscocapillary model of slide coating can be constructed and its range of validity are governed by the limitation of the approximations used: small inclination of film thickness, low capillary number, and low Reynolds number. The approximation worsen at the bead zone, as expected, where in the 1D viscocapillary model it was assumed to be a static pool and in a realistic coating operation, it is not so. The results show that viscocapillary model are accurate only at low capillary numbers and small gap-to-thickness ratio.

On the basis of on our observations, we conclude that a 1D slide coating model that can be applied at high capillary and Reynolds number cannot be derived. The reason is that the flow in the bead region is far from a static pool. We propose an efficient model by inserting N-S theory at a suitably defined bead region, as depicted in Figure 19, to link the film profile equations down the slide and up the web. The hybrid model is the most efficient approach to study slide coating flows and the operating limits of the process. It takes advantage of the asymptotic model where it is valid and relies on the full 2D model where the flow is far from rectilinear. This model is under construction.

Literature Cited

1. Christodoulou KN, Scriven LE. The fluid mechanics of slide coating. *J Fluid Mech*. 1989;208:321–354.
2. Youn SI, Kim SY, Shin DM, Lee JS, Jung HW, Hyun JC. A review on viscocapillary models of pre-metered coating flows. *Korea Aust Rheol J*. 2006;18:209–215.
3. Galehouse D, Colt J. Simplified analytical solutions of the free fluid surfaces associated with slide coating. *AICHE Annual Meeting*, Atlanta, GA, March 12, 1984.
4. Hens J, van Abbenyen W. Slide coating. In: Kistler SF, Schweizer PM, editors. *Liquid Film Coating*. London, UK: Chapman and Hall, 1997:427–462.
5. Nagashima K. Slide coating flow: splice passage. Master's Thesis, University of Minnesota, Minnesota, 1993.

6. Nagashima K. Viscocapillary modelling of slide coating flow. *Ind Coat Res*. 2004;5:81–106.
7. Jung HW, Lee JS, Hyun JC, Kim SJ, Scriven LE. Simplified modeling of slide-fed curtain coating flow. *Korea Aust Rheol J*. 2004;16:227–233.
8. Higgins BG, Scriven LE. Interfacial shape and evolution equations for liquid films and other viscocapillary flows. *Ind Eng Chem Fund*. 1979;18:208–215.
9. Kheshgi HS, Kistler SF, Scriven LE. Rising and falling film flows: viewed from first order approximations. *Chem Eng Sci* 1992;47: 683–694.
10. Vinokur M. On one-dimensional stretching functions for finite-difference calculations. *J Comput Phys*. 1983;50:215–234.
11. de Santos JM. Two-phase cocurrent downflow through constricted passages. Ph.D. Thesis, University Microfilms International, Ann Arbor, MI, 1991.
12. Bixler NE. Stability of coating flow. Ph.D. Thesis, University Microfilms International, Ann Arbor, MI, 1982.
13. Romero OJ, Suszynski WJ, Carvalho MS, Scriven LE. Low-flow limit in slot coating of dilute solutions of high molecular weight polymer. *J Non-Newton Fluid Mech*. 2004;118:137–156.

Manuscript received Sept. 5, 2008, revision received Dec. 19, 2008, and final revision received Jan. 15, 2009.